Expression Profiling after Retinal Detachment and Reattachment: A Possible Role for Aquaporin-0

Rafal Farjo,[1,2] *Ward M. Peterson,*[3] *and Muna I. Naash*[1]

Purpose. Retinal detachment (RD) is associated with acute visual loss caused by anatomic displacement of the photoreceptors and with chronic visual loss/disturbance caused by retinal remodeling and photoreceptor cell death, which may occur even after successful reattachment. The $P2Y_2$ receptor agonist INS37217 improves the rate of retinal reattachment in animal models of induced RD, and has been shown to also significantly enhance the rate of ERG recovery in a mouse model of RD. The identification of genes modulated by INS37217 may allow further drug discovery for treating RD and edema.

Methods. To identify genes involved in RD and subsequent reattachment, a retinal microarray screen was performed using a mouse model of RD in the presence or absence of INS37217.

Results. Ninety-two genes were identified as differentially expressed across three time points, most of which were upregulated in the presence of this agonist. Furthermore, it was shown that RD alters the expression of aquaporin-0 (AQP-0), and this modulation is prevented by treatment with INS37217. The presence of AQP-0 in retinal bipolar cells was also demonstrated, whereas it was previously thought to be specific to the lens. Mice lacking functional alleles of AQP-0 had a phototransduction deficit as assessed by electroretinography; however, their photoreceptor structure was normal, indicative of a problem with signal transmission between neurons.

Conclusions. This study establishes the genes involved in RD and reattachment, and also demonstrates for the first time a physiologically significant role for AQP-0 in retinal function. (*Invest Ophthalmol Vis Sci.* 2008;49:511–521) DOI:10.1167/iovs.07-1013

Retinal detachment (RD) is a sight-threatening condition that occurs when the neural retina physically separates from the retinal pigment epithelium (RPE). In clinical and animal models of RD, photoreceptors undergo apoptotic cell death and the retina undergoes secondary changes such as gliosis, hypertrophy, and synaptic remodeling.[1–3] RD-induced changes in retinal gene and protein expression are thought to play important roles in stimulating stress-induced intrinsic neuroprotective mechanisms in the retina and in delaying or compromising the recovery of vision even after successful anatomic reattachment.[4–7]

Nearly complete RD can be induced in mice by transretinal injection of saline into the subretinal space. This procedure creates a detachment similar to rhegmatogenous detachments in humans, whereby a tear in the retina allows fluid to accumulate between the RPE and the retina. We have shown that the retina spontaneously reattaches within 1 to 2 days after detachment, but this reattachment is associated with massive retinal in-foldings.[8] Complete reattachment occurs 7 days after the initial detachment, but retinal function, as measured by electroretinography (ERG), is only approximately 50% of normal even though the retina appears to be anatomically reattached and morphologically intact. This resolution of RD in our animal model more closely mimics the exudative form of human RD. In humans, fluid accumulates between the RPE and the retina without any tear or break. Even at 14 days after detachment, the ERG is only approximately 60% of normal, and full recovery is not observed electroretinographically until 2 months after the initial detachment. We also demonstrated that the administration of the $P2Y_2$ receptor agonist INS37217 in this RD model resulted in almost complete recovery of retinal ERG function by 10 days after detachment, presumably through stimulating fluid reabsorption across the RPE and perhaps through some other direct neurorestorative effects on the retina.[8,9] Because of the relatively long time lag between full anatomic reattachment (approximately 7 days) and full recovery of ERG function (approximately 2 months), this model represents a useful system for studying the delayed recovery of neurosensory function after physical traumatic injury to the retina. Although this model does not perfectly mimic one specific form of RD, it may provide insight into the mechanisms underlying the delayed or incomplete recovery of normal visual function frequently seen in RD patients after otherwise successful reattachment of the retina.

In this study, we evaluated the effects of RD and spontaneous reattachment in the absence and presence of INS37217 on retinal gene expression to determine which genes are involved in response to an induced detachment and subsequent reattachment occurring in response to a pharmacologic agent known to hasten RD and recovery. Here we identified several genes involved in these response pathways that appeared to be likely candidates for accelerating the process of reattachment and perhaps ERG recovery. Based on our microarray screen, we evaluated the potential role for aquaporin-0 (AQP-0) as a direct mediator involved in the response to and recovery from RD. Expression of AQP-0 was previously thought to be specific to the lens, but we demonstrate its expression in retinal cells. Furthermore, we show that the loss of AQP-0 in mice has deleterious effects on the transmission of phototransduction signals, indicating an essential physiological function for AQP-0 in the retina.

From the [1]Department of Cell Biology, University of Oklahoma Health Sciences Center, Oklahoma City, Oklahoma; and [3]Inspire Pharmaceuticals Inc., Durham, North Carolina.

[2]Present address: Charlesson LLC, Oklahoma City, Oklahoma.

Supported in part by Inspire Pharmaceuticals Inc., the National Institutes of Health (Grant NEI-EY10609), the Oklahoma Center for the Advancement of Science and Technology, and the Foundation Fighting Blindness.

Submitted for publication August 6, 2007; revised October 15, 2007; accepted December 19, 2007.

Disclosure: **R. Farjo**, Inspire Pharmaceuticals Inc. (F); **W.M. Peterson**, Inspire Pharmaceuticals Inc. (E, F); **M.I. Naash**, Inspire Pharmaceuticals Inc. (F)

The publication costs of this article were defrayed in part by page charge payment. This article must therefore be marked "*advertisement*" in accordance with 18 U.S.C. §1734 solely to indicate this fact.

Corresponding author: Muna I. Naash, Department of Cell Biology, University of Oklahoma Health Sciences Center, 940 Stanton L. Young Boulevard, BMSB 781, Oklahoma City, OK 73104; muna-naash@ouhsc.edu.

TABLE 1. Genes Differentially Expressed 2 Hours after Detachment

Gene Symbol	Gene Name	Gene Chip Fold Change (INS/SAL)	qRT-PCR Fold Change (INS/SAL)
Top2b	Topoisomerase (DNA) II beta	+2.49	+6.45
Aplp2	Amyloid beta (A4) precursor-like protein 2	+2.24	—
Crygc	Crystallin, gamma C	+2.22	+2.50
Atp6v0a1	ATPase, H+ transporting, lysosomal V0 subunit a isoform 1	+2.19	—
Usp12	Ubiquitin-specific protease 12	+2.00	+3.28
1200003l10Rik	RIKEN cDNA 1200003l10	+2.00	—
Hspa1b	Heat-shock protein 1B	+2.00	+10.14
Ywhag	3-Monooxgenase/tryptophan 5-monooxgenase activation protein, gamma polypeptide	+1.97	+14.70
Bfsp1	Beaded filament structural protein in lens-CP94	+1.96	+4.08
Mbd1	Methyl-CpG binding domain protein 1	+1.96	—
Kif5c	Kinesin family member 5C	+1.95	+6.64
Aqp0	Aquaporin 0	+1.93	+3.25
Dscr1	Down syndrome critical region homolog 1 (human)	+1.91	—
Cpeb4	Cytoplasmic polyadenylation element binding protein 4	+1.90	+2.96
Npn3	Neoplastic progression 3	+1.90	—
Crygb	Crystallin, gamma B	+1.89	—
Rs1h	Retinoschisis 1 homolog (human)	+1.89	+10.48
Hspa1a/Hspa1b	Heat-shock protein 1A/heat-shock protein 1B	+1.89	—
Cryga	Crystallin, gamma A	+1.87	+2.19
Dct	Dopachrome tautomerase	−1.87	—
Dio2	Deiodinase, iodothyronine, type II	−1.94	—
Hba-a1	Hemoglobin alpha, adult chain 1	−1.95	−2.86
Nr4a1	Nuclear receptor subfamily 4, group A, member 1	−2.04	−2.15
Egr2	Early growth response 2	−2.05	−9.80
Dcn	Decorin	−2.20	—
Hbb-b1	Hemoglobin, beta adult major chain	−2.21	−5.29
Fosb	FBJ osteosarcoma oncogene B	−2.21	−8.92
Tyrp1	Tyrosinase-related protein 1	−2.24	−4.34
Si	Silver	−2.32	—
Alas2	Aminolevulinic acid synthase 2, erythroid	−2.59	−3.67

MATERIALS AND METHODS

Animal Use and Care

Balb/cJ mice were used for microarray experiments and were obtained from the Jackson Laboratories (Bar Harbor, ME). $AQP^{-/-}$ (CatFr), also obtained from the Jackson Laboratories, were on a C57BL/6 background. All experiments and animal maintenance procedures were approved by the local Institutional Animal Care and Use Committee (Oklahoma City, OK) and conformed to the guidelines on the care and use of animals adopted by the Society for Neuroscience and contained in the ARVO Statement for the Use of Animals in Ophthalmic and Vision Research.

Subretinal Injections and RNA Isolation

Subretinal injections were performed as previously described.[8] Briefly, 1 μL saline or 1 μL saline/10 μM INS37217 was delivered to the subretinal space in Balb/cJ mice by transvitreal injection. This procedure creates a retinal hole that is self-sealing because material delivered will not diffuse into the vitreous.[9] Mock injections consisting solely of a corneal puncture with no RD were also performed as a control. Mice were humanely killed at 2 hours, 24 hours, or 7 days after injection, and their retinas were harvested directly into reagent (Trizol; (Invitrogen, Carlsbad, CA). For each time point, three separate pools of at least five retinas were collected for saline- and INS37217-injected mice. After tissue homogenization, total RNA was isolated as previously described and was purified by a method for total isolation of RNA (RNeasy column; Qiagen, Valencia, CA).

Gene Chip Hybridization and Analyses

We used each RNA pool (each containing more than five retinas) for hybridization (GeneChip; Affymetrix, Santa Clara, CA), giving a total of three biological replicates for each treatment at each time point. For each hybridization (GeneChip; Affymetrix), we labeled 7 μg total RNA according to the manufacturer's specifications. Gene chips (MOE_430A; Affymetrix) were hybridized with 15 μg cRNA for 16 hours at 45° in a hybridization oven (Hybridization Oven 640; Affymetrix) rotating at 60 rpm. Washing, staining, and scanning were performed according to the manufacturer's specifications using a fluidics station and a scanner (Fluidics Station 450 and GeneChip Scanner 3000; Affymetrix). Data sets were normalized using the robust multivariate algorithm (RMA) implemented in data analysis software (Spotfire DecisionSite for Microarray Analysis; TIBCO Software, Palo Alto, CA). Resultant $\log_2$ expression values were used to make expression comparisons. Because the RMA algorithm is known to compress data sets, we set a threshold for differential expression at 1.8-fold change. All microarray data have been submitted to the National Center for Biotechnology Information Gene Expression Omnibus in compliance with MIAME guidelines under the series accession number GSE5766 (http://www.ncbi.nlm.nih.gov/geo//query/acc.cgi?acc=GSE5766).

Quantitative RT-PCR

Quantitative (q) RT-PCR was performed as previously described.[10] Briefly, total RNA was DNAse treated with RNase-free DNAse I (Promega, Madison, WI), and reverse transcription was performed using oligo-dT primer and reverse transcriptase (Superscript III; Invitrogen). Primers for all genes were designed to span introns so as to avoid amplification from genomic DNA. A complete list of primers used in this study is available in Supplementary Table S1, online at http://www.iovs.org/cgi/content/full/49/2/511/DC1. qRT-PCR was performed in triplicate on each cDNA sample (iCycler; Bio-Rad, Hercules, CA), and ΔcT values were calculated against the neuronal housekeeping gene hypoxanthine phosphoribosyltransferase (*Hprt*). *Hprt* was

TABLE 2. Genes Differentially Expressed 24 Hours after Detachment

Gene Symbol	Gene Name	Gene Chip Fold Change (INS/SAL)	qRT-PCR Fold Change (INS/SAL)
Slfn4	Schlafen 4	+6.70	+4.06
S100a9	S100 calcium binding protein A9 (calgranulin B)	+3.07	+4.43
S100a8	S100 calcium binding protein A8 (calgranulin A)	+2.80	—
Oasl2	2′-5′ oligoadenylate synthetase-like 2	+2.75	—
Ifi202a	Interferon-activated gene 202	+2.64	+6.43
C920025E04Rik	RIKEN C920025E04 gene	+2.53	—
Cfb	Complement factor B	+2.51	+8.73
Isg12	Interferon-stimulated gene 12	+2.49	+12.30
Lcn2	Lipocalin 2	+2.46	+48.73
C3	Complement component 3	+2.43	+6.24
H28	Histocompatibility 28	+2.42	—
Mmp3	Matrix metalloproteinase 3	+2.41	+57.96
Slfn3///Slfn4	Schlafen 3 /// schlafen 4	+2.38	—
Rsad2	Radical S-adenosyl methionine domain containing 2	+2.35	—
Ifi44	Interferon-induced protein 44	+2.32	+16.08
Ifit1	Interferon-induced protein with tetratricopeptide repeats 1	+2.28	+4.13
Ifit3	Interferon-induced protein with tetratricopeptide repeats 3	+2.26	—
Chi3l1	Chitinase 3-like 1	+2.24	+3.77
Prg1	Proteoglycan 1, secretory granule	+2.22	—
Trim30	Tripartite motif protein 30	+2.22	+2.11
Plac8	Placenta-specific 8	+2.21	—
Arg1	Arginase 1, liver	+2.19	+10.28
Saa3	Serum amyloid.A 3	+2.14	—
B2m	Beta-2 microglobulin	+2.11	—
Tnfaip9	Tumor necrosis factor, alpha-induced protein 9	+2.10	+14.67
Ms4a11/Ms4a6d	Membrane-spanning 4-domains, subfamily A, member 11///membrane-spanning 4-domains, subfamily A, member 6D	+2.08	—
Tgfbi	Transforming growth factor, beta induced	+2.07	+6.20
Rtp4	Receptor transporter protein 4	+2.01	—
Cd53	CD53 antigen	+1.99	+4.92
Gbp4	Guanylate nucleotide binding protein 4	+1.98	—
Ly6a	Lymphocyte antigen 6 complex, locus A	+1.96	—
Lrg1	Leucine-rich alpha-2-glycoprotein 1	+1.89	+2.04
Arr3	Arrestin 3, retinal	−1.87	−2.58
Hba-a1	Hemoglobin alpha, adult chain 1	−2.09	−3.05

assigned an arbitrary expression level of 10,000, and relative gene expression values were calculated by Relative Expression = $10{,}000/2^{\Delta cT}$, where ΔcT = (*Gene* cT − *Hprt* cT). This was repeated with each of the three total RNA pools isolated for each treatment at the specified time point; the mean expression value is presented with the SD. Fold changes presented in Tables 1 to 3 were calculated by the equation Fold change = $2^{\Delta\Delta cT}$, where the ΔΔcT represents the difference of mean ΔcTs between saline (SAL)- or INS37217 (INS)-injected samples. Statistical significance was determined using ANOVA with Bonferroni post hoc multiple pairwise comparison tests (PRISM; GraphPad Software, San Diego, CA). Disassociation curve analysis was performed on all PCR products to confirm proper amplification.

Immunoblotting and Immunoprecipitation Analysis

Protein extracts were prepared from tissue samples homogenized on ice and solubilized overnight at 4°C in solubilization buffer (50 mM Tris-HCl, [pH 7.5], 100 mM NaCl, 5 mM EDTA, 1% Triton X-100, 0.05% SDS, 2.5% glycerol, and 1.0 mM phenylmethylsulfonyl fluoride). After determination of protein concentrations, 50 μg (or 1 μg for lens extracts) was loaded on a 10% SDS-PAGE gel and transferred to polyvinylidene difluoride membrane for subsequent immunoblotting. After blocking in 5% milk/TBST for 30 minutes at room temperature (RT), primary antibodies were applied in 5% milk/TBST for 2 hours at RT, followed by three washes in TBST for 10 minutes. Horseradish peroxidase-conjugated secondary antibodies were applied at 1:25,000 in TBST for 50 minutes at RT, followed by four washes in TBST for 15 minutes and subsequent detection (SuperSignal Dura; Pierce, Rockford, IL). Primary antibodies and dilutions were rabbit–anti-AQP-0 (1:1000; Alpha Diagnostic International, San Antonio, TX); rabbit–anti-γ-crystallin (1:1000; generous gift from Usha Andley); mouse–anti-β-actin (1:10,000; Sigma, St. Louis, MO). For immunoprecipitation, 100 μg retinal protein extracts or 1 μg lens protein extracts were immunoprecipitated with 5 μg goat–anti-γ-crystallin (Santa Cruz Biotechnology Inc., Santa Cruz, CA) overnight with rotation at 4°. Samples were then incubated with protein G-Sepharose beads (Sigma) in a volume of 200 μL at 4°C for 1 hour. After adsorption, the beads were washed with solubilization buffer four times, and bound proteins were eluted with 2× sample buffer, followed by gel electrophoresis and immunoblot analysis with anti–AQP-0 or anti–γ-crystallin. For image acquisition and analysis, an image station (CF 440; Eastman Kodak, Rochester, NY) was used. Pixel quantification was carried out with molecular imaging software (Eastman Kodak). No detectable bands were observed after immunoblotting with anti–AQP-0 in the presence of a peptide competitor.

Immunohistochemistry

Eyes from adult mice were fixed in 4% paraformaldehyde/PBS for 12 to 16 hours at RT. Cryosections or paraffin sections were obtained as previously described and were blocked in 5% BSA/PBS, 0.5% Triton-X, for 30 minutes at RT.[8,10] Slides were briefly washed with PBS and incubated with the primary antibody in 1× BSA/PBS, 0.5% Triton-X for 2 hours at RT, followed by a brief wash in PBS and incubation with the secondary antibody in 1× BSA/PBS, 0.5% Triton-X, for 30 minutes at

TABLE 3. Genes Differentially Expressed 7 Days after Detachment

Gene Symbol	Gene Name	Gene Chip Fold Change (INS/SAL)	qRT-PCR Fold Change (INS/SAL)
Arg1	Arginase 1, liver	+9.42	+24.38
Col1a2	Procollagen, type I, alpha 2	+4.99	+30.84
Col1a1	Procollagen, type I, alpha 1	+4.76	—
Spp1	Secreted phosphoprotein 1	+4.01	+12.67
Col3a1	Procollagen, type III, alpha 1	+3.90	+27.08
Ccl6	Chemokine (C-C motif) ligand 6	+3.87	—
Fbln2	Fibulin 2	+3.07	+8.15
Serpina3n	Serine (or cysteine) proteinase inhibitor, clade A, member 3N	+2.91	—
Fn1	Fibronectin 1	+2.67	+6.29
Tgfbi	Transforming growth factor, beta induced	+2.63	+8.11
Fcgr2b	Fc receptor, IgG, low affinity IIb	+2.56	—
Postn	Periostin, osteoblast-specific factor	+2.52	—
Bgn	Biglycan	+2.37	+3.97
Lzp-s	P lysozyme structural	+2.33	+4.12
F13a1	Coagulation factor XIII, A1 subunit	+2.13	—
Lilrb4	Leukocyte immunoglobulin-like receptor, subfamily B, member 4	+2.09	—
Cxcl4	Chemokine (C-X-C motif) ligand 4	+2.09	+10.24
H19	H19 fetal liver mRNA	+2.05	—
Tagln	Transgelin	+2.01	—
Prg1	Proteoglycan 1, secretory granule	+2.00	+8.90
Ecm1	Extracellular matrix protein 1	+1.98	+3.54
Col5a1	Procollagen, type V, alpha 1	+1.97	—
C3ar1	Complement component 3a receptor 1	+1.96	—
Timp1	Tissue inhibitor of metalloproteinase 1	+1.96	+2.95
H2-Aa	Histocompatibility 2, class II antigen A, alpha	+1.95	—
Ptprc	Protein tyrosine phosphatase, receptor type, C	+1.93	—
Cd68	CD68 antigen	+1.91	+2.55
C3	Complement component 3	+1.87	+4.72

RT. After a brief wash in PBS, mounting medium with DAPI (Vectashield; Vector Laboratories, Burlingame, CA) was applied, and the slide was coverslipped. Primary antibodies and dilutions were rabbit–anti-AQP-0 (1:1000; Alpha Diagnostic International); mouse–anti-PKCα (1:2000; generous gift of Yousif Hannun); mouse–anti-Goα (1:1000; Chemicon, Temecula, CA); guinea pig–anti-vGlut1 (1:2500; Chemicon). Secondary antibodies were anti–mouse fluorescent dye (Alexa 488, 1:500; Invitrogen), anti–rabbit fluorescent dye (Alexa 555, 1:500; Invitrogen), and anti–guinea pig fluorescent dye (Alexa 647, 1:500; Invitrogen). Images were acquired with a camera (C-4742; Hamamatsu, Hamamatsu, Japan) through Olympus objectives (UPlanSApo; Olympus, Tokyo, Japan) on an upright microscope (BX62; Olympus) equipped with a spinning disc confocal unit. Projection images were performed with Olympus software (Slidebook, version 4). No detectable signal was observed after immunohistochemistry with anti–AQP-0 in the presence of a peptide competitor.

Electroretinography

Scotopic and photopic ERG was performed as previously described.[8,10] Significance was determined using one-way analysis of variance (ANOVA) and post hoc tests using Bonferroni pairwise comparisons (PRISM, version 3.02; GraphPad).

RESULTS

We conducted a microarray screen to identify genes involved in promoting faster resolution of RD and recovery of function. RD was induced in Balb/cJ mice by transvitreal subretinal injections of 1 μL saline or of 1 μL of 10 μM INS37217/saline to cause detachment and to expedite the rate of recovery. We performed this study at three time points: 2 hours after injection to identify early-response genes; 24 hours after detachment, when the retina reattached but was still grossly misfolded; and 7 days after detachment, when the misfolding was resolved but retinal function was merely 50% of wild-type function. We used gene chips (MOE_430A GeneChips; Affymetrix) to evaluate the expression levels of more than 22,000 probe sets in several biological replicates of saline-injected (SAL) or INS37217-injected (INS) retinas during this study. After microarray hybridization, analysis, and data normalization, we identified genes at each time point showing a microarray fold change of $\geq$1.8-fold between SAL- and INS-injected samples. We performed qRT-PCR on a subset of the genes identified as differentially expressed at each time point to validate the microarray results. Of the 92 genes modulated throughout the three time points, 52 of 52 examined by qRT-PCR confirmed the change in expression levels observed with the microarray, but the level of change was often underestimated by the microarray data.

Two hours after detachment, we identified 30 genes that demonstrated differential expression between INS- and SAL-injected retinas (Table 1). Of these, the upregulation of retinoschisis-1 (RS1) is a likely factor in forcing physical cohesion throughout the retina. RS1 is a secreted protein that maintains adhesions between photoreceptor, bipolar, and Müller glial cells throughout the retina.[11,12] Furthermore, mutations in RS1 cause retinoschisis, a disease in which retinal cells come apart from each other, causing vision loss.[13] An upregulation of several antiapoptotic genes—including heat shock protein-1A, heat shock protein-1B, and 14-3-3-gamma, and a downregulation of the proapoptotic genes nuclear receptor subfamily 4-A1, FBJ murine osteosarcoma viral oncogene homolog B, and early growth response-2—was observed in the INS-treated samples, consistent with our earlier findings that this compound reduces apoptosis in the detached retina.[14–19] Finally, we observed an upregulation of aquaporin-0 (AQP-0) and γ-crystallin proteins, known to serve as chaperone molecules for AQP-0.[20,21] Given that the aquaporin family of proteins is well characterized and is known to be involved in solute transfer,[22]

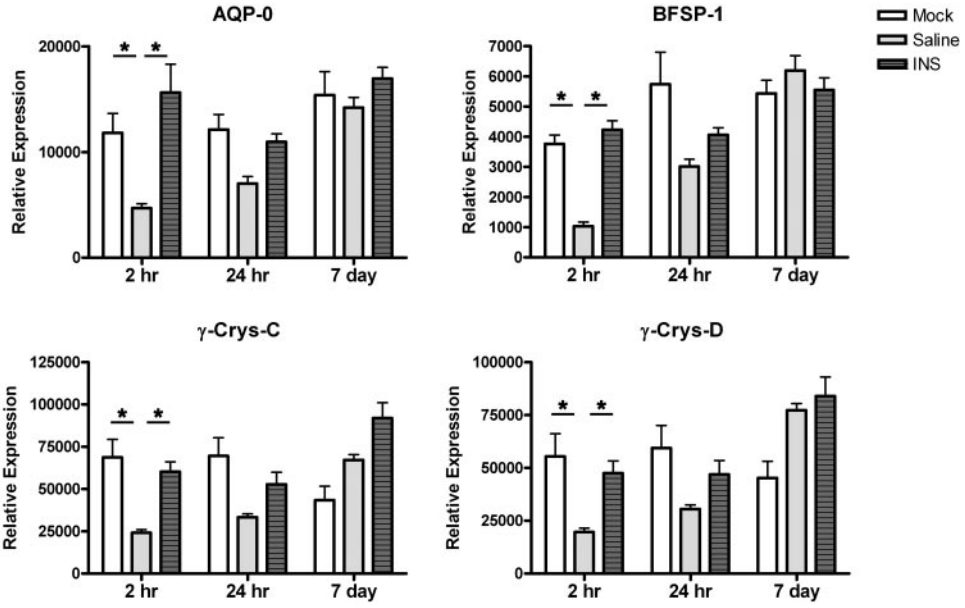

FIGURE 1. Expression profile of selected genes differentially expressed 2 hours after injection. qRT-PCR was performed on AQP-0, BFSP-1, γ-Crys-C, and γ-Crys-D in mock-, SAL-, and INS-injected retinas at 2 hours, 24 hours, and 7 days after injection. For all four genes, a similar expression pattern 2 hours after injection was noticeable. The expression of these genes was maintained at mock-injected levels in the INS-detached retinas; however, the levels were markedly decreased in the SAL-detached retinas at this time point. In addition, in the case of every gene examined here, the expression profile for SAL-injected samples gradually increased throughout the three time points. $^*P < 0.05$, ANOVA with Bonferroni post hoc multiple pairwise comparison tests.

we sought to further characterize the role of this protein in the retina and during the reattachment process. The time course expression profile of these genes suggested that they are indeed early-response molecules because their expression was restored to basal levels by 24 hours after injection (Supplementary Fig. S1, http://www.iovs.org/cgi/content/full/49/2/511/DC1). We examined four of these genes throughout the three time points with qRT-PCR and included mock-injected retinas to assess the effect of detachment on gene expression. SAL detachment appeared to cause downregulation of these genes in AQP-0, beaded structural filament protein (BFSP)-1, γ-Crys-C, and γ-Crys-D, but the INS-detached retinas maintained wild-type expression levels (Fig. 1).

Twenty-four hours after detachment, we identified 34 genes that demonstrated differential expression between INS- and SAL-injected retinas, and 32 of these exhibited higher expres-

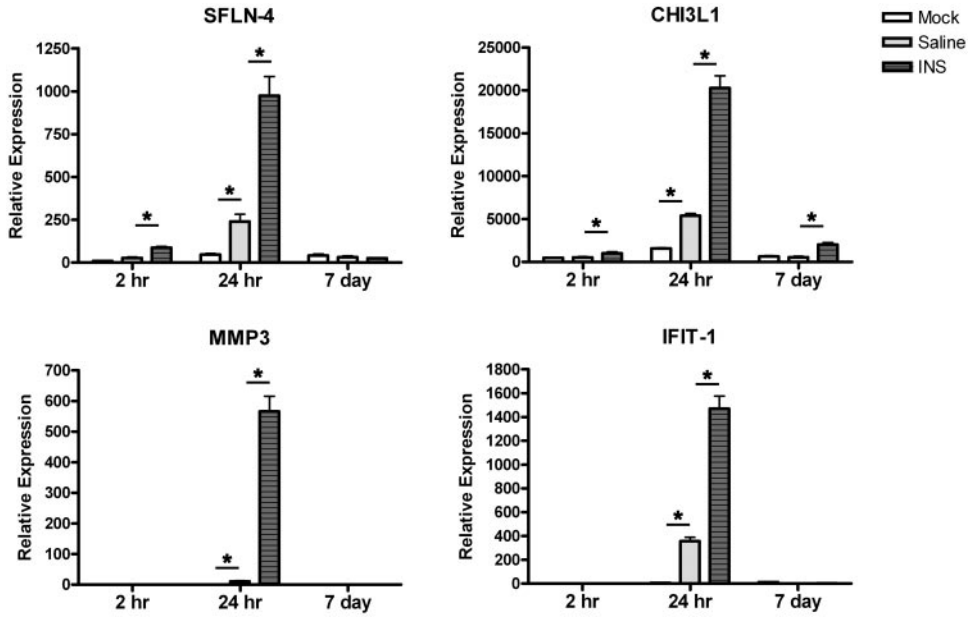

FIGURE 2. Expression profile of selected genes differentially expressed 24 hours after injection. qRT-PCR was performed on Schlafen-4 (SFLN-4), Chitinase-3-like-1 (CHI3L1), matrix metalloproteinase-3 (MMP3), and interferon-induced transcript-1 (IFIT1) in mock-, SAL-, and INS-injected retinas at 2 hours, 24 hours, and 7 days after injection. In all cases, the expression of these genes was induced by SAL detachment by 24 hours; however, the level of induction was greatly increased in the INS-detached retinas. Both *SFLN-4* and *CHI3L1* showed higher levels of expression in the INS-detached retinas even at 2 hours after injection. The expression of these genes in the INS-injected retinas peaked at the 24-hour time point, as did the other genes differentially expressed at this time point as depicted in Supplementary Figure S2, http://www.iovs.org/cgi/content/full/49/2/511/DC1. By 7 days after injection, the expression of these genes had been restored to near mock-injected levels. Mean ± SD expression values are plotted. $^*P < 0.05$, ANOVA with Bonferroni post hoc multiple pairwise comparison tests.

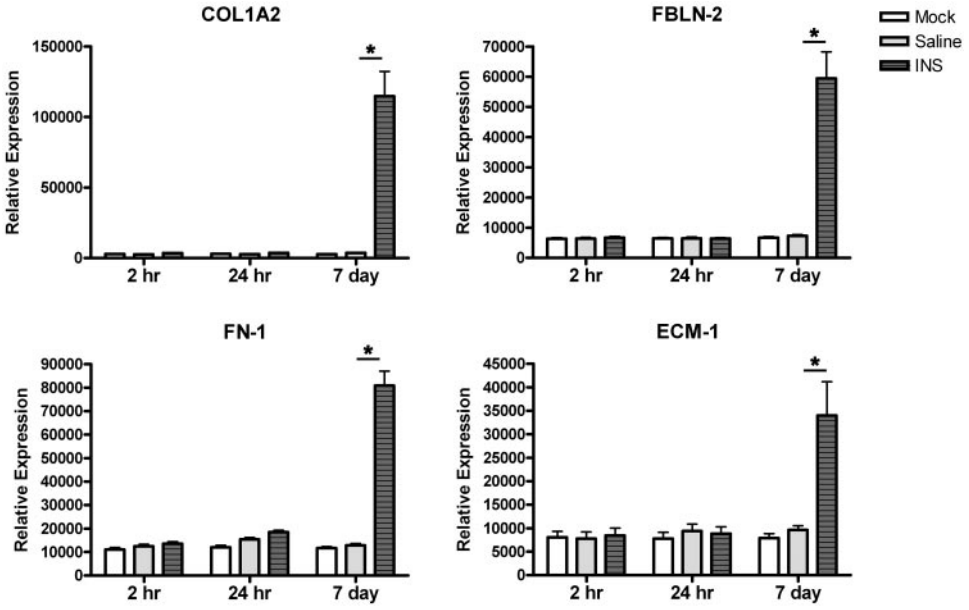

FIGURE 3. Expression profile of selected genes differentially expressed 7 days after injection. qRT-PCR was performed on procollagen type-1-α-2 (COL1A2), fibulin-2 (FBLN2), fibronectin-1 (FN1), and extracellular matrix protein 1 (ECM1) in mock-, SAL-, and INS-injected retinas at 2 hours, 24 hours, and 7 days after injection. The expression of these four genes was constant throughout the mock- and SAL-injected samples; however, a dramatic increase in expression is detected in the INS-detached retinas 7 days after injection, consistent with the microarray data. Upregulation of these genes likely depicted the enhanced cellular remodeling that occurs to restore structure and function in the INS-detached retinas. Mean ± SD expression values are plotted. $^*P < 0.01$, ANOVA with Bonferroni post hoc multiple pairwise comparison tests.

sion in the INS-detached samples (Table 2). In almost all cases, the differentially expressed genes at 24 hours were nearly unchanged from SAL-detached retinas at the 2 hours and 7 days (Supplementary Fig. S2, http://www.iovs.org/cgi/content/full/49/2/511/DC1). It is probable that upregulated calgranulin A and calgranulin B are downstream effectors in response to activation of the $P2Y_2$ receptor, which is proposed to trigger Ca^{2+} efflux from endoplasmic reticulum stores.[9] At this time point, we also observed an upregulation of several genes induced by interferon. Although the precise function of these genes in the retina is unclear, a recent report suggests that the presence of interferon in the eye can reduce a damaging inflammatory response.[23] Of the genes confirmed with qRT-PCR, matrix metalloproteinase 3 (MMP3) showed the highest level of upregulation. MMP3 is involved in extracellular matrix remodeling and, specifically, the breakdown of ECM components, which may implicate this process during detachment resolution.[24] Lastly, we detected a downregulation of arrestin-3, which is involved in the deactivation of opsin in cone photoreceptors and could potentiate phototransductive signaling.[25] SFLN-4, CHI3L1, MMP3, and IFIT1, when examined with the use of qRT-PCR, displayed similar expression profiles (Fig. 2). In each case, expression of the gene was induced by SAL detachment at 24 hours; however, the level of induction was several times higher in the INS-detached retinas. By 7 days after injection, the expression of these genes in the detached retinas was restored to levels nearly equal to those of mock-injected retinas.

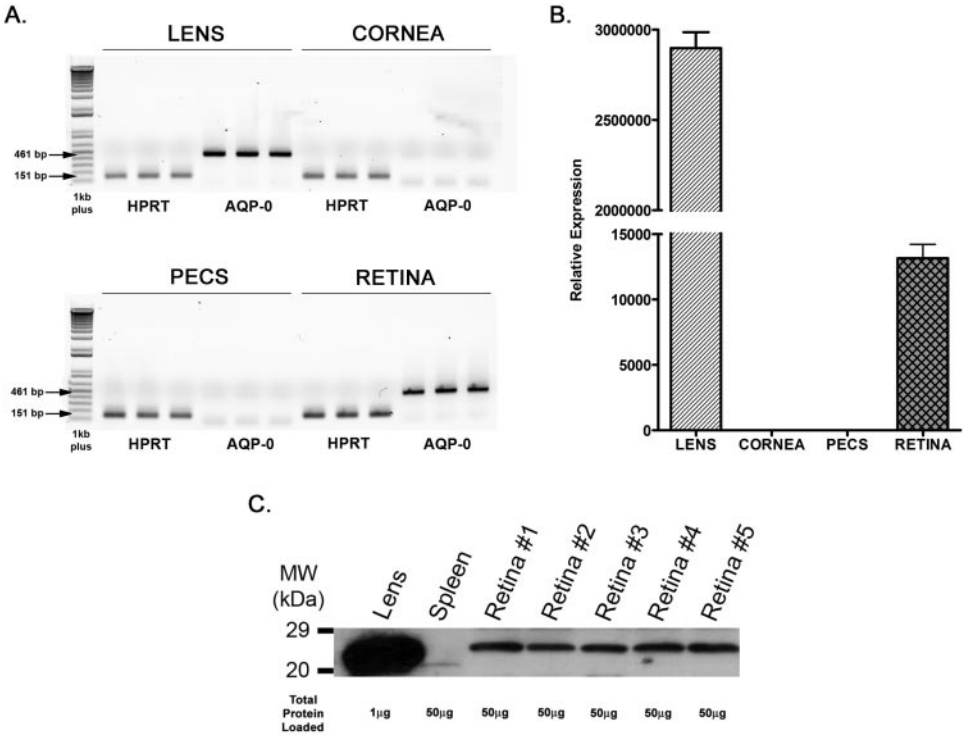

FIGURE 4. AQP-0 mRNA and protein are expressed in the murine retina. (**A**) Lens, cornea, pigment epithelium/choroid/sclera (PECS), and retina were carefully dissected from mouse eyes and assessed for AQP-0 mRNA expression. In all tissues, amplification of the control gene *HPRT* was observed, but in AQP-0, amplification was detected only in the lens and the retina. (**B**) qRT-PCR analysis on these same tissue samples revealed that the retinal expression of AQP-0 was nearly 250-fold less than that observed in the lens. (**C**) Immunoblot analysis was performed using anti-AQP-0 on lens, spleen, and five retinal extracts from mice. A band at 26 kDa was detected in lens and all five retinal protein extracts but not in the spleen sample. The amount of protein loaded is represented below each lane. The abundance of AQP-0 protein in the retina compared with the lens appeared to be proportional to the mRNA level.

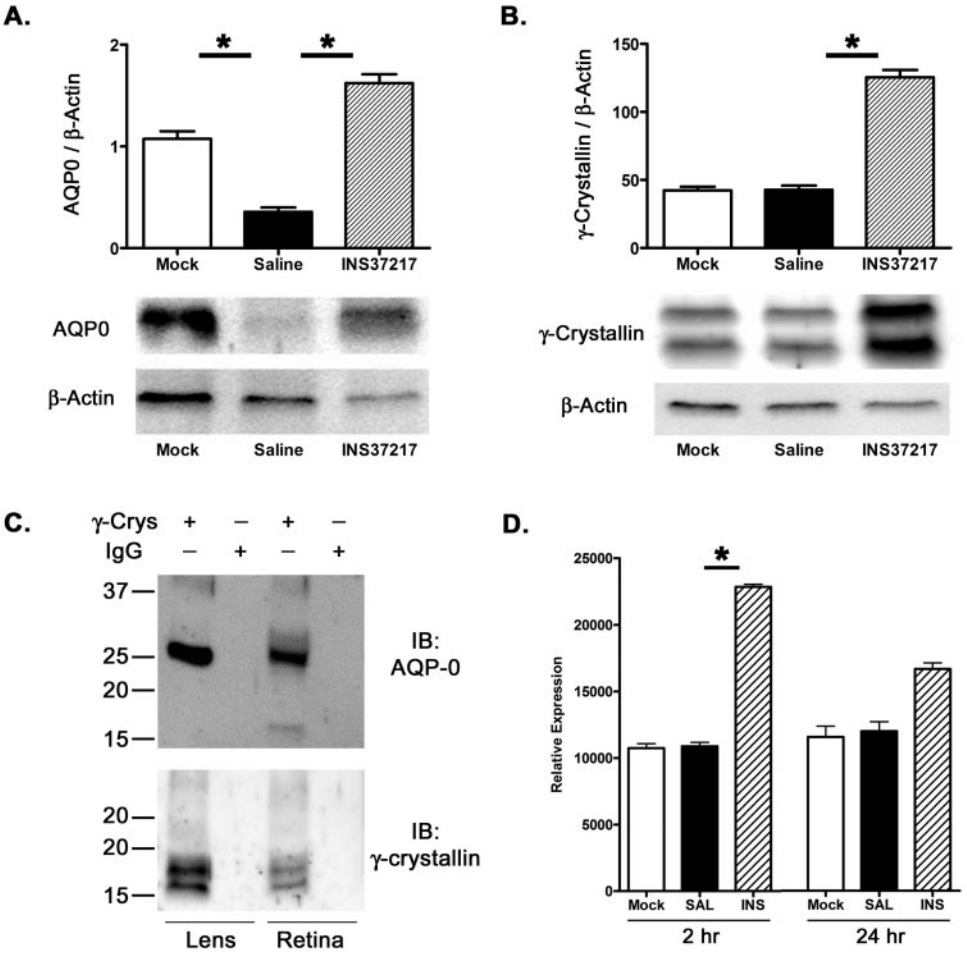

FIGURE 5. AQP-0 and γ-crystallin expression after delivery of INS37217. Quantitative immunoblot analysis was performed on retinal extracts isolated 2 hours after mock, SAL, or INS injection and normalized to the levels of β-actin. (**A**) AQP-0 levels were higher in the INS-detached retina compared with mock- and SAL-injected samples. (**B**) A similar increase in the amount of γ-crystallin proteins was also observed. (**C**) Immunoprecipitation was performed on lens and retinal protein extracts with goat–anti-γ-crystallin or goat-IgG followed by immunoblot analysis with anti–AQP-0 or anti–γ-crystallin. AQP-0 was absent in control lanes but present in immunoprecipitates from the retina and lens, suggesting protein interactions in the retina similar to those in the lens. (**D**) qRT-PCR analysis of mice retina that underwent intravitreal delivery of saline or the P2Y2 agonist INS37217. Compared with mock-injected controls, the SAL-injected retinas showed no significant change in the levels of AQP-0. However, administration of INS37217 caused an upregulation of AQP-0 mRNA 2 hours after injection that was reduced by 24 hours after injection, demonstrating that activation of the $P2Y_2$ receptor alone is sufficient to upregulate AQP-0. Densitometry/expression values are plotted (mean ± SD). $^*P < 0.05$, ANOVA with Bonferroni post hoc multiple pairwise comparison tests.

Seven days after detachment, we identified 28 genes that demonstrated differential expression between INS- and SAL-injected retinas, and all these were upregulated in the INS-detached samples (Table 3). We observed significant upregulation of several genes known to be involved in extracellular matrix remodeling and cell adhesion, including multiple procollagens, biglycan, fibulin-2, fibronectin-1, and extracellular matrix protein-1.[26–29] Also of note, we observed an upregulation of tissue inhibitor of MMP1, which is a known inhibitor of MMP3 and could be part of a negative feedback pathway to reduce the level of MMP3 after its upregulation 24 hours after INS detachment.[24] Temporal expression profiles of these differentially expressed genes show that many were unchanged 2 hours after detachment but that they gradually increased to peak expression levels 7 days after detachment (Supplementary Fig. S3, http://www.iovs.org/cgi/content/full/49/2/511/DC1). When examined with qRT-PCR, COL1A2, FBLN2, FN1, and ECM1 displayed equal expression levels between mock-injected, SAL-, and INS-detached retinas 2 hours and 24 hours after injection. A spike in expression was detected in the INS-detached retinas after 7 days (Fig. 3).

The aquaporin family of proteins is composed of 11 members, all involved in solute transfer.[22] AQP-0 is also known as the major intrinsic protein of the lens and functions as a water channel.[30] AQP-0 was thought to be specifically expressed in the lens. We sought to examine its expression in the retina because we had identified it in our microarray screen. The lens, cornea, pigment epithelium/choroid/sclera (PECS), and retina were dissected from several mouse eyes and assessed for AQP-0 mRNA by RT-PCR (Fig. 4A). AQP-0 mRNA was solely detected in the lens and the retina, and quantification of this revealed expression levels in the lens nearly 250-fold higher than in the retina (Fig. 4B). To further confirm retinal expression of AQP-0, we performed immunoblot analysis on several retinal protein isolates (Fig. 4C). AQP-0 protein was detected in all five retinal samples examined, albeit at levels greatly reduced compared with the lens.

Because the microarray screen identified that AQP-0 and γ-crystallin mRNAs were upregulated in the INS-treated retinas compared with the SAL-injected retinas, we sought to determine whether this upregulation corresponded to an increase in protein levels. RD was created in mice by injection of SAL or INS, and the retinas were harvested into three individual pools 2 hours after injection. Immunoblot analysis was then performed on each tissue pool to examine the levels of AQP-0 and γ-crystallin proteins (Fig. 5A, 5B). The upregulation of AQP-0 and γ-crystallin proteins was apparent in the INS-injected samples after band intensities were quantified and normalized to the levels of β-actin. Given that these proteins are known to interact in the lens,[20,21] we performed coimmunoprecipitation assays on retinal extracts. AQP-0 protein was detected in lens and retinal samples after immunoprecipitation with an antibody recognizing γ-crystallins but not with a normal IgG antibody (Fig. 5C). Attempts to show the reciprocal associations were unsuccessful because the anti–AQP-0 antibody could not immunoprecipitate AQP-0. Lastly, we examined whether the upregulation of AQP-0 was dependent on the presence of RD, INS37217, or both (Fig. 5D). INS37217 was delivered to the retina in the absence of detachment by means of intravitreal injection, and retinas were assessed for AQP-0 mRNA levels at 2 and 24 hours after injection. AQP-0 mRNA levels were unchanged after intravitreal injection of saline but showed a more

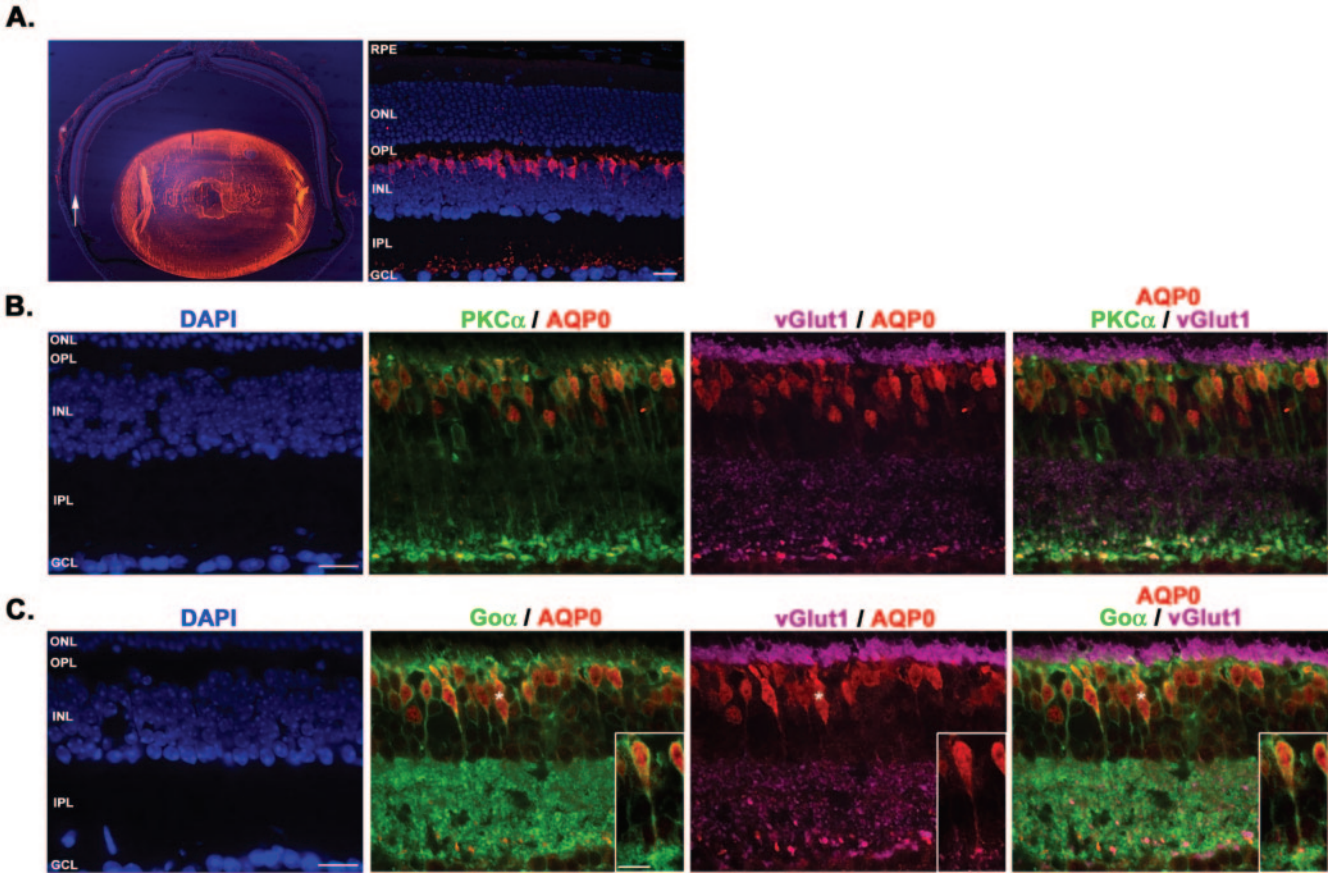

FIGURE 6. Localization of AQP-0 protein in the murine retina. (**A**) Immunohistochemistry was performed with anti–AQP-0 on paraffin-embedded eye sections, and nuclei were counterstained with DAPI. AQP-0 staining is evident throughout the lens; however, a band of immunoreactivity is noticeable in the retina (*white arrow*). At higher magnification, this staining is apparent around cell bodies and dendrites in the outer part of the inner nuclear layer. AQP-0 immunoreactivity is also detected in structures close to the ganglion cell layer. Scale bar, 20 μm. (**B**) To determine the specific cell types that expressed AQP-0, immunohistochemistry was performed on retinal cryosections with anti–AQP-0, anti-PKCα to label rod bipolar cells, and anti-vGlut1 to label synaptic terminals. Nuclei were counterstained with DAPI. Confocal images were acquired, and the projection of the image stack is depicted. AQP-0 is expressed in rod bipolar cells as colocalization of AQP-0, and PKCα staining is evident at the cell membrane in many cells. Most AQP-0, however, appears confined to the cell body. Anti–AQP-0 staining is apparent around cells not labeled by anti-PKCα. AQP-0 immunoreactivity near the ganglion cell layer did colocalize with anti-PKCα and anti-vGlut1, demonstrating that AQP-0 was expressed in the synaptic terminals of rod bipolar cells. Scale bar, 20 μm. (**C**) Immunohistochemistry was performed on retinal cryosections with anti-AQP-0, anti-Goα to label cone and rod bipolar cells, and anti-vGlut1 to label synaptic terminals. Nuclei were counterstained with DAPI. Every cell labeled by anti–AQP-0 was also labeled by anti-Goα, indicating that AQP-0 was expressed only in rod and cone ON-bipolar cells of the inner nuclear layer. *Insets*: projection image at higher magnification of a single bipolar cell present in the original image stack (*white asterisk*). Based on the location of the cell body and synaptic terminal, this was likely a type 1 to 4 cone ON-bipolar cell.[32] AQP-0 expression was detected at the plasma membrane, throughout the soma, and in the axon of this cell. Thus, AQP-0 was expressed in rod bipolar cells and a subset of cone on-bipolar cells in the murine retina. Scale bars, 20 μm (**A–C**), 10 μm (*insets*). ONL, outer nuclear layer; OPL, outer plexiform layer; IPL, inner plexiform layer.

than twofold increase after delivery of INS37217. Hence, activation of the $P2Y_2$ receptor by this agonist acts to upregulate AQP-0, regardless of a physiological insult.

To localize AQP-0 in the retina, we performed immunohistochemistry on retinal sections with an anti–AQP-0 antibody (Fig. 6). At low magnification, AQP-0 immunoreactivity is apparent throughout the lens, but two bands of immunoreactivity are apparent throughout the retina. On examination at higher magnification, AQP-0 immunoreactivity is confined to a set of cells within the inner nuclear layer and around structures resembling synaptic terminals in the inner plexiform layer near the ganglion cells (Fig. 6A). To define the cell types expressing AQP-0, we performed colocalization studies using antibodies to mark various types of second-order neurons in the retina. We performed immunohistochemistry on retinal cryosections with anti-PKCα to label rod bipolar cells, anti-vglut1 to label all bipolar cell terminals, anti-Goα to label all ON-type cone and rod bipolar cells, and anti-AQP-0. AQP-0 immunoreactivity colocalized with PKCα staining in most of the AQP-0–positive cells in the inner nuclear layer (Fig. 6B). Furthermore, the staining observed near the ganglion cell layer (GCL) colocalized with anti-PKCα and anti-vglut1, demonstrating that AQP-0 is expressed in the soma and dendrites of the rod bipolar cells and in the synaptic terminals. This staining pattern was also detected in macaque retina (data not shown). When we used anti-Goα, every cell containing AQP-0 was also positive for Goα, a marker for cone and rod bipolar cells.[31] We also observed AQP-0 in the soma and axons of bipolar cells whose axons terminate in the inner-half of the inner plexiform layer (Fig. 6C). This labeling pattern is characteristic of type 1 to 4 cone bipolar cells because other bipolar cells, including rod bipolars, terminate their axons more closely to the GCL.[32] These data demonstrate that AQP-0 is expressed in rod and cone bipolar cells of the retina.

To delineate the involvement of AQP-0 in phototransduction, we examined the response of AQP-0–deficient mice to light by means of electroretinography (Fig. 7). We obtained Cat^{Fr} mice, which harbor a transposon long terminal repeat in intron 3 of the

AQP-0 gene.[33] This sequence insertion contains a splice acceptor site, causing the formation of a chimeric protein that is unable to be expressed on the plasma membrane. This appears to be a gain-of-function mutation, and these animals develop cataracts in a manner similar to that of AQP-0 knockout mice generated by gene trapping.[33,34] Scotopic ERG analysis of postnatal day (P) 30 mice revealed significantly decreased scotopic a- and b-waves in $AQP0^{-/-}$ mice that were nearly 75% those in wild-type C57BL/6 controls, but no significant decrease was observed in $AQP0^{+/-}$ mice. When cone photoreceptor function was assessed with photopic ERG, both $AQP0^{+/-}$ and $AQP0^{-/-}$ mice showed significant loss of function. These results suggest a role for AQP-0 in phototransductive signaling.

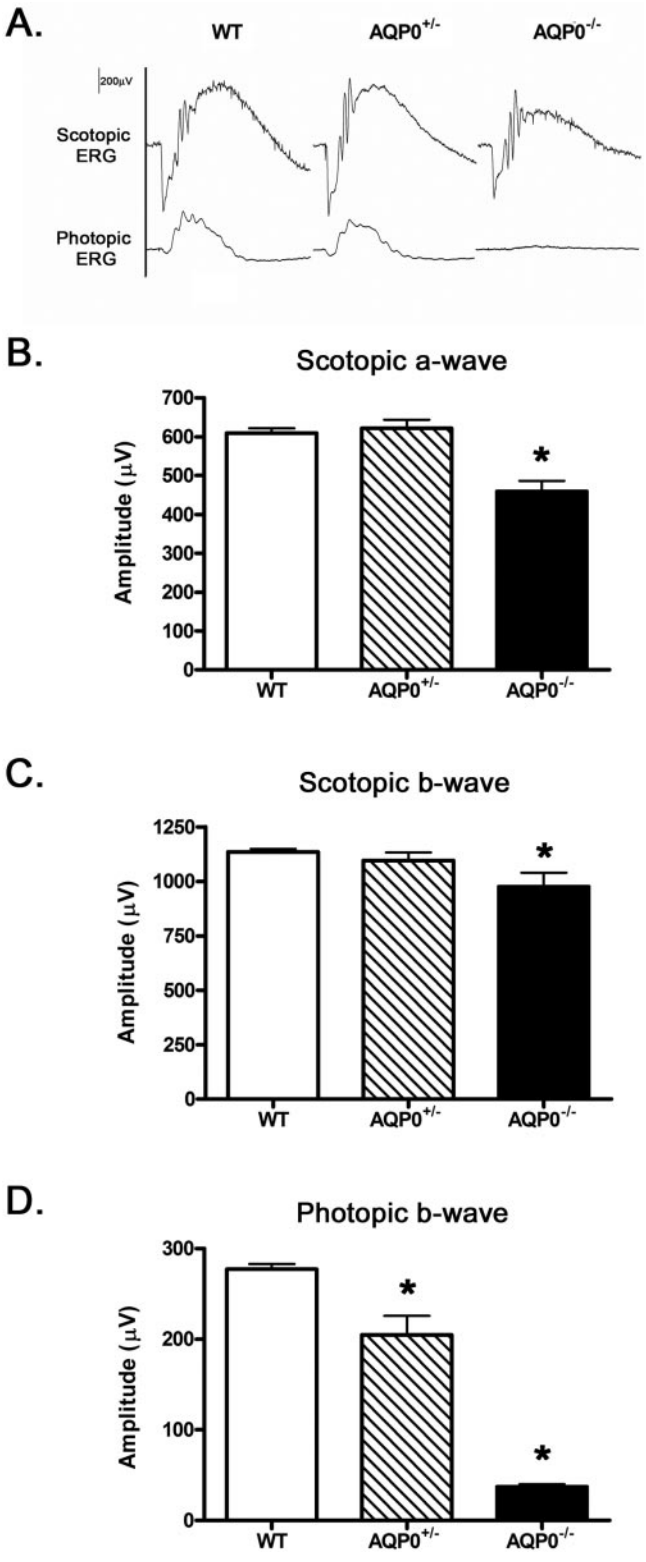

Discussion

Herein we have identified changes in gene expression that are associated with RD and spontaneous reattachment in an animal model, in the absence and presence of pharmacologic agent INS37217, known to enhance retinal reattachment and recovery of retinal function. Most of these differentially expressed genes appeared to regulate retinal apoptosis, cellular adhesions, and extracellular remodeling. Of particular interest was the novel identification of AQP-0 expression in the retina and its potential role in retinal response to detachment. We also provide additional evidence for the involvement of AQP-0 in the transmission of phototransduction signals.

Because this model undergoes spontaneous resolution of RD, it is different from other RD models in which sodium hyaluronate is used to create a long-lasting detachment. The creation of RD by the injection of saline is comparable to rhegmatogenous RD in humans, but this spontaneous resolution is more typical of exudative RD that is clinically observed. Using stringent criteria, we identified 92 genes that were differentially expressed among the three time points, and 52 of 52 genes examined with qRT-PCR demonstrated a greater than twofold change. Because the robust multivariate algorithm used for gene chip normalization is known to compress the data set,[35,36] it is likely that lowering our threshold for genes with modulated expression would have identified additional genes involved in the resolution process; however, it is also likely that some of these would be false-positives if examined with qRT-PCR.

Throughout the three time points examined in this study, most of the differentially expressed genes were upregulated in detached retinas in the presence of INS37217. The genes identified at 2 hours after injection likely represented early-response genes associated with acute RD. The upregulation of RS1 is noteworthy. This secreted protein can decrease morphologic disruption because it is involved in maintaining cellular adhesions throughout the retina.[11,13] Previous studies of RD have noted an activation of apoptotic pathways after experimental detachment.[4,6,7] At this time point, we also observed the upregulation of antiapoptotic genes and the downregulation of proapoptotic genes, correlating with our previous evidence that fewer TUNEL-positive cells are present in the detached retina treated with INS37217.[8] Last, we noted that INS37217 maintained basal levels of AQP-0, γ-crystallins, and BFSP1, which are all known to interact together in the lens to facilitate fluid movement.[20,21,37] At this stage, it is unknown whether INS37217 directly upregulates expression of

Figure 7. AQP-0–deficient mice have impaired retinal function. Scotopic and photopic ERG analyses were performed on P30 AQP0-deficient mice and compared with wild-type littermate controls. (**A**) Representative scotopic and photopic waveforms from wild-type (C57Bl/6), $AQP0^{+/-}$, and $AQP0^{-/-}$ mice. (**B**, **C**) Scotopic a- and b-wave amplitudes were diminished to nearly 75% of wild-type controls in $AQP0^{-/-}$ mice, but no statistically significant change was observed in $AQP0^{+/-}$ mice. (**C**) Photopic b-wave amplitudes were greatly reduced in $AQP0^{-/-}$ and $AQP0^{+/-}$ mice, indicating the requirement of two functional alleles of AQP-0 to provide proper transmission of the cone photoreceptor-derived signal. Mean ± SD ERG amplitudes are plotted. $^{*}P < 0.05$, ANOVA with Bonferroni post hoc multiple pairwise comparison tests.

these molecules or prevents their downregulation, which occurred naturally with detachment in our experimental model. Twenty-four hours after injection, we observed a tremendous upregulation of MMP3, a known mediator of cellular remodeling. We also detected several interferon-induced transcripts that could play a protective role in preventing immune cell infiltration. An upregulation of complement component c3 and tripartite motif protein 30 was also detected. Although we did not observe any immune cell infiltration in our previous studies, we cannot rule out the possibility that this $P2Y_2$ agonist may cause an ocular immune response. In addition, 24 hours after injection, we detected an upregulation of transforming growth factor β-induced, which modulates the aggregation of extracellular matrix genes such as collagen and biglycan.[38] These two genes and several other additional extracellular matrix components, such as fibronectin 1 and proteoglycan 1, which are likely representatives of enhanced cellular remodeling, were upregulated 7 days after injection. Also noteworthy was the upregulation of the MMP3 antagonist TIMP1, possibly part of a negative feedback loop to reduce MMP3 activity in response to the high levels observed 24 hours after injection. In sum, these data provide evidence regarding the specific genes affected during the enhanced resolution of RD, and they suggest a number of potential therapeutic targets worthy of further study.

AQP-0 is known as the major intrinsic protein of the lens. Together with the γ-crystallins and BFSP, it is responsible for extruding water from the lens. The crystal structure of AQP-0 from lens samples further identified that this molecule forms a closed water pore across membranes, mediated by three localized interactions.[30] Another study demonstrated that AQP-0 functions as a cellular adhesion molecule because C-terminal cleavage causes an increase in its adhesive properties.[39] Based on these functions and our microarray data, we hypothesized that this molecule could play a major role in enhancing structural and functional recovery after RD. Several studies have provided tremendous insight into the disease-causing mutations, regulation, biochemical interactions, and structure of this gene, but its expression has never been reported in any tissue except the lens.[37,40–44] Here we provide strong evidence that AQP-0 mRNA and protein are indeed present in the retina (Fig. 4). Expression levels in the retina are nearly 250-fold lower than in the lens, likely contributing to the disregard of its presence in the retina. We demonstrated that AQP-0 and γ-crystallins could coimmunoprecipitate from retinal extracts, as has been observed in lens cells.[20,21] In the murine retina, γ-crystallin expression is observed throughout the inner nuclear layer (INL).[45] When examined using immunohistochemistry, we detected AQP-0 in the dendrites, soma, and axons of rod and cone bipolar cells in the INL of the retina. This signal was only observed in "ON-type" rod and cone bipolar cells because all AQP-0–positive cells were labeled by anti-Goα. Furthermore, we observed strong AQP-0 immunoreactivity in the synaptic terminals of rod bipolar cells. Although the aquaporin family of genes is highly homologous, it is unlikely that we detected other aquaporins in the retina because of the specificity of the C-terminal peptide of AQP-0 originally used to generate the antibody. Previous studies have shown aquaporin-4 expression in the retina,[46] but this was observed in Müller cells and astrocytes in the optic nerve, a localization pattern not observed with our antibody. Other studies have shown aquaporin-1 and aquaporin-9 expression in rat photoreceptor and amacrine cells,[47,48] yet this labeling pattern was different from what we observed with the AQP-0 antibody used in this study. Furthermore, competitive immunoblotting and immunohistochemistry performed in the presence of the peptide used to generate the antibody resulted in the lack of any detectable signal from the lens and retina (data not shown).

The localization pattern observed for AQP-0 suggests that it may be intimately involved in the process of synaptic transmission, cellular adhesion to maintain proper cell contacts for phototransductive signaling, and rapid water movement to facilitate electrical signal transduction. To provide evidence for this proposed function, we examined electroretinographically the retinal physiology of mice deficient in wild-type AQP-0. These analyses demonstrated a deficit of nearly 25% in the levels of the rod photoreceptor-derived a- and b-wave. However, mice containing one functional allele of AQP-0 showed ERG amplitudes unchanged from those of wild-type littermate controls. Furthermore, cone photoreceptor-derived b-wave levels were almost completely depressed by the loss of functional AQP-0. It is unlikely that these results were biased by the presence of cataracts because P30 $AQP^{+/-}$ mice also displayed significantly lower cone b-wave amplitude and do not develop cataracts until P45 to P60. We detected no global abnormalities while examining the ultrastructure of the photoreceptors in AQP-0–deficient mice (data not shown), suggesting that the functional deficit is a result of flawed signal transmission between higher-order neurons. These results suggest a role for the importance of AQP-0 for normal retinal function.

Because AQP-0 expression was increased after intravitreal administration of INS37217, we sought to provide direct evidence that AQP-0 was intimately involved in the resolution process by creating RD in $AQP^{-/-}$ mice in the presence or absence of INS37217, with the hypothesis that this $P2Y_2$ agonist would not promote faster recovery to the same degree as observed in wild-type mice. Unfortunately, we were unable to perform subretinal injections in these mice because they had congenital cataracts, making our delivery method and assessment of detachment impossible. Future studies using siRNA to knock down AQP-0 concurrently with the creation of RD in wild-type mice may provide this direct evidence. Nevertheless, the data presented here suggest a role for AQP-0 in normal retinal physiology. Further examination of the other genes identified in our microarray screen may provide the basis for the rational development of therapeutics for treating RD and other physiological insults, such as macular edema, when expedited fluid movement is required for the maintenance of proper retinal morphology and phototransductive signaling.

Acknowledgments

The authors thank Jeff Skaggs, Carla Hansens, Barbara A. Nagel, and Ashley Ezzell for technical assistance; May Nour for her technical assistance during the initial stages of the study; Krysten Farjo for stimulating discussions; and Usha Andley and Yousif Hannun for the generous gift of their antibodies used in this study.

References

1. Fisher SK, Lewis GP, Linberg KA, Verardo MR. Cellular remodeling in mammalian retina: results from studies of experimental retinal detachment. *Prog Retin Eye Res*. 2005;24:395–431.
2. Sethi CS, Lewis GP, Fisher SK, et al. Glial remodeling and neural plasticity in human retinal detachment with proliferative vitreoretinopathy. *Invest Ophthalmol Vis Sci*. 2005;46:329–342.
3. Lewis GP, Sethi CS, Linberg KA, Charteris DG, Fisher SK. Experimental retinal reattachment: a new perspective. *Mol Neurobiol*. 2003;28:159–175.
4. Zacks DN, Han Y, Zeng Y, Swaroop A. Activation of signaling pathways and stress-response genes in an experimental model of retinal detachment. *Invest Ophthalmol Vis Sci*. 2006;47:1691–1695.
5. Rex TS, Fariss RN, Lewis GP, Linberg KA, Sokal I, Fisher SK. A survey of molecular expression by photoreceptors after experimental retinal detachment. *Invest Ophthalmol Vis Sci*. 2002;43:1234–1247.
6. Cook B, Lewis GP, Fisher SK, Adler R. Apoptotic photoreceptor degeneration in experimental retinal detachment. *Invest Ophthalmol Vis Sci*. 1995;36:990–996.

7. Lewis GP, Linberg KA, Geller SF, Guerin CJ, Fisher SK. Effects of the neurotrophin brain-derived neurotrophic factor in an experimental model of retinal detachment. *Invest Ophthalmol Vis Sci*. 1999;40:1530–1544.
8. Nour M, Quiambao AB, Peterson WM, Al-Ubaidi MR, Naash MI. P2Y(2) receptor agonist INS37217 enhances functional recovery after detachment caused by subretinal injection in normal and rds mice. *Invest Ophthalmol Vis Sci*. 2003;44:4505–4514.
9. Maminishkis A, Jalickee S, Blaug SA, et al. The P2Y(2) receptor agonist INS37217 stimulates RPE fluid transport in vitro and retinal reattachment in rat. *Invest Ophthalmol Vis Sci*. 2002;43:3555–3566.
10. Farjo R, Skaggs JS, Nagel BA, et al. Retention of function without normal disc morphogenesis occurs in cone but not rod photoreceptors. *J Cell Biol*. 2006;173:59–68.
11. Molday LL, Hicks D, Sauer CG, Weber BH, Molday RS. Expression of X-linked retinoschisis protein RS1 in photoreceptor and bipolar cells. *Invest Ophthalmol Vis Sci*. 2001;42:816–825.
12. Grayson C, Reid SN, Ellis JA, et al. Retinoschisin, the X-linked retinoschisis protein, is a secreted photoreceptor protein, and is expressed and released by Weri-Rb1 cells. *Hum Mol Genet*. 2000; 9:1873–1879.
13. Molday RS. Focus on molecules: retinoschisin (RS1). *Exp Eye Res*. 2007;84:227–228.
14. Lee JS, Lee JJ, Seo JS. HSP70 deficiency results in activation of c-Jun N-terminal kinase, extracellular signal-regulated kinase, and caspase-3 in hyperosmolarity-induced apoptosis. *J Biol Chem*. 2005;280:6634–6641.
15. Clemons NJ, Buzzard K, Steel R, Anderson RL. Hsp72 inhibits Fas-mediated apoptosis upstream of the mitochondria in type II cells. *J Biol Chem*. 2005;280:9005–9012.
16. Sekimoto T, Fukumoto M, Yoneda Y. 14–3-3 suppresses the nuclear localization of threonine 157-phosphorylated p27(Kip1). *EMBO J*. 2004;23:1934–1942.
17. Steel R, Doherty JP, Buzzard K, Clemons N, Hawkins CJ, Anderson RL. Hsp72 inhibits apoptosis upstream of the mitochondria and not through interactions with Apaf-1. *J Biol Chem*. 2004;279: 51490–51499.
18. Unoki M, Nakamura Y. EGR2 induces apoptosis in various cancer cell lines by direct transactivation of BNIP3L and BAK. *Oncogene*. 2003;22:2172–2185.
19. Kim SO, Ono K, Tobias PS, Han J. Orphan nuclear receptor Nur77 is involved in caspase-independent macrophage cell death. *J Exp Med*. 2003;197:1441–1452.
20. Fan J, Donovan AK, Ledee DR, Zelenka PS, Fariss RN, Chepelinsky AB. γE-crystallin recruitment to the plasma membrane by specific interaction between lens MIP/aquaporin-0 and γE-crystallin. *Invest Ophthalmol Vis Sci*. 2004;45:863–871.
21. Fan J, Fariss RN, Purkiss AG, et al. Specific interaction between lens MIP/aquaporin-0 and two members of the gamma-crystallin family. *Mol Vis*. 2005;11:76–87.
22. Verkman AS. Role of aquaporin water channels in eye function. *Exp Eye Res*. 2003;76:137–143.
23. Fukushima A, Yamaguchi T, Ishida W, Fukata K, Udaka K, Ueno H. Mice lacking the IFN-gamma receptor or fyn develop severe experimental autoimmune uveoretinitis characterized by different immune responses. *Immunogenetics*. 2005;57:337–343.
24. Nagase H, Woessner JF Jr. Matrix metalloproteinases. *J Biol Chem*. 1999;274:21491–21494.
25. Yarfitz S, Hurley JB. Transduction mechanisms of vertebrate and invertebrate photoreceptors. *J Biol Chem*. 1994;269:14329–14332.
26. Wiberg C, Heinegard D, Wenglen C, Timpl R, Morgelin M. Biglycan organizes collagen VI into hexagonal-like networks resembling tissue structures. *J Biol Chem*. 2002;277:49120–49126.
27. Argraves WS, Greene LM, Cooley MA, Gallagher WM. Fibulins: physiological and disease perspectives. *EMBO Rep*. 2003;4:1127–1131.
28. Monaghan E, Gueorguiev V, Wilkins-Port C, McKeown-Longo PJ. The receptor for urokinase-type plasminogen activator regulates fibronectin matrix assembly in human skin fibroblasts. *J Biol Chem*. 2004;279:1400–1407.
29. Fujimoto N, Terlizzi J, Brittingham R, Fertala A, McGrath JA, Uitto J. Extracellular matrix protein 1 interacts with the domain III of fibulin-1C and 1D variants through its central tandem repeat 2. *Biochem Biophys Res Commun*. 2005;333:1327–1333.
30. Gonen T, Sliz P, Kistler J, Cheng Y, Walz T. Aquaporin-0 membrane junctions reveal the structure of a closed water pore. *Nature*. 2004;429:193–197.
31. Vardi N. Alpha subunit of Go localizes in the dendritic tips of ON bipolar cells. *J Comp Neurol*. 1998;395:43–52.
32. Ghosh KK, Bujan S, Haverkamp S, Feigenspan A, Wassle H. Types of bipolar cells in the mouse retina. *J Comp Neurol*. 2004;469:70–82.
33. Shiels A, Mackay D, Bassnett S, Al-Ghoul K, Kuszak J. Disruption of lens fiber cell architecture in mice expressing a chimeric AQP0-LTR protein. *FASEB J*. 2000;14:2207–2212.
34. Shiels A, Bassnett S, Varadaraj K, et al. Optical dysfunction of the crystalline lens in aquaporin-0-deficient mice. *Physiol Genomics*. 2001;7:179–186.
35. Millenaar FF, Okyere J, May ST, van Zanten M, Voesenek LA, Peeters AJ. How to decide? Different methods of calculating gene expression from short oligonucleotide array data will give different results. *BMC Bioinformatics*. 2006;7:137.
36. Irizarry RA, Bolstad BM, Collin F, Cope LM, Hobbs B, Speed TP. Summaries of Affymetrix GeneChip probe level data. *Nucleic Acids Res*. 2003;31:e15.
37. Lindsey Rose KM, Gourdie RG, Prescott AR, Quinlan RA, Crouch RK, Schey KL. The C terminus of lens aquaporin 0 interacts with the cytoskeletal proteins filensin and CP49. *Invest Ophthalmol Vis Sci*. 2006;47:1562–1570.
38. Reinboth B, Thomas J, Hanssen E, Gibson MA. Beta Ig-H3 interacts directly with biglycan and decorin, promotes collagen VI aggregation, and participates in ternary complexing with these macromolecules. *J Biol Chem*. 2006;281:7816–7824.
39. Gonen T, Cheng Y, Kistler J, Walz T. Aquaporin-0 membrane junctions form upon proteolytic cleavage. *J Mol Biol*. 2004;342: 1337–1345.
40. Ball LE, Garland DL, Crouch RK, Schey KL. After translational modifications of aquaporin 0 (AQP0) in the normal human lens: spatial and temporal occurrence. *Biochemistry*. 2004;43:9856–9865.
41. Berry V, Francis P, Kaushal S, Moore A, Bhattacharya S. Missense mutations in MIP underlie autosomal dominant 'polymorphic' and lamellar cataracts linked to 12q. *Nat Genet*. 2000;25:15–17.
42. Golestaneh N, Fan J, Fariss RN, Lo WK, Zelenka PS, Chepelinsky AB. Lens major intrinsic protein (MIP)/aquaporin 0 expression in rat lens epithelia explants requires fibroblast growth factor-induced ERK and JNK signaling. *J Biol Chem*. 2004;279:31813–31822.
43. Gonen T, Cheng Y, Sliz P, et al. Lipid-protein interactions in double-layered two-dimensional AQP0 crystals. *Nature*. 2005;438: 633–638.
44. Yu XS, Yin X, Lafer EM, Jiang JX. Developmental regulation of the direct interaction between the intracellular loop of connexin 45.6 and the C terminus of major intrinsic protein (aquaporin-0). *J Biol Chem*. 2005;280:22081–22090.
45. Xi J, Farjo R, Yoshida S, Kern TS, Swaroop A, Andley UP. A comprehensive analysis of the expression of crystallins in mouse retina. *Mol Vis*. 2003;9:410–419.
46. Nagelhus EA, Veruki ML, Torp R, et al. Aquaporin-4 water channel protein in the rat retina and optic nerve: polarized expression in Muller cells and fibrous astrocytes. *J Neurosci*. 1998;18:2506–2519.
47. Iandiev I, Pannicke T, Reichel MB, Wiedemann P, Reichenbach A, Bringmann A. Expression of aquaporin-1 immunoreactivity by photoreceptor cells in the mouse retina. *Neurosci Lett*. 2005;388:96–99.
48. Iandiev I, Biedermann B, Reichenbach A, Wiedemann P, Bringmann A. Expression of aquaporin-9 immunoreactivity by catecholaminergic amacrine cells in the rat retina. *Neurosci Lett*. 2006;398:264–267.